Available online at www.sciencedirect.com
ScienceDirect
Acta Materialia 58 (2010) 6554–6564
Acta MATERIALIA
www.elsevier.com/locate/actamat

Simulations of stress-induced twinning and de-twinning: A phase field model

ShenYang Hu [a,*], Chuck H. Henager Jr. [a], LongQing Chen [b]

[a] Pacific Northwest National Laboratory, 902 Battelle Boulevard, Richland, WA 99352, USA
[b] Department of Materials Science and Engineering, The Pennsylvania State University, University Park, PA 16802, USA

Received 29 June 2010; received in revised form 13 August 2010; accepted 17 August 2010

Abstract

Twinning in certain metals or under certain conditions is a major plastic deformation mode. Here we present a phase field model to describe twin formation and evolution in a polycrystalline fcc metal under loading and unloading. The model assumes that twin nucleation, growth and de-twinning is a process of partial dislocation nucleation and slip on successive habit planes. Stacking fault energies, energy pathways (γ surfaces), critical shear stresses for the formation of stacking faults and dislocation core energies are used to construct the thermodynamic model. The simulation results demonstrate that the model is able to predict the nucleation of twins and partial dislocations, as well as the morphology of the twin nuclei, and to reasonably describe twin growth and interaction. The twin microstructures at grain boundaries are in agreement with experimental observation. It was found that de-twinning occurs during unloading in the simulations, however, a strong dependence of twin structure evolution on loading history was observed.

Keywords: Phase field method; Partial dislocation; Deformation twin; Polycrystal deformation

1. Introduction

Deformation twinning is a major plastic deformation mode in some cubic and in most non-cubic materials [1–4]. For example, in hcp crystals, where deformation by slip along some directions either is not possible or requires very high stresses, twinning is a dominant deformation mechanism. Although plastic deformation predominantly occurs via dislocation nucleation and slip in coarse grained fcc metals and alloys with medium to high stacking fault energies, deformation twinning becomes important in nanocrystalline materials as grain sizes decreases [5–9]. Twin formation during crystal growth from the melt due to crucible contact stresses or growth stresses can be problematic in the processing of single crystals, such as CdTeZn growth via the vertical gradient freeze method [10,11]. A fundamental understanding of the effect of microstructure, defects and external stresses on twin nucleation and growth is helpful in designing advanced or improving existing materials and materials processing methods.

Experiments and atomistic simulations show that deformation twinning in nanocrystalline fcc metals forms and evolves via partials dislocations emitted from grain boundaries [5–9]. The stacking fault energy and energy pathways are predicted using first principle calculations [12–14]. Molecular dynamics (MD) simulations have been successfully used to investigate how grain boundary structure influences dislocation nucleation and in examining the twinning mechanisms [9,15,16]. Stacking fault core fields in fcc metals have been analyzed by MD simulations and continuous models [17]. The critical twinning stress was estimated using a continuous mechanical model [3,12], which suggests that the shear stress on the habit plane and slip direction of the twin controls twin nucleation. In addition, one of the commonly accepted mechanisms in both coarse grained and nanocrystalline fcc metals is that a twin nucleates and evolves via the nucleation and slip

* Corresponding author. Tel.: +1 509 371 6928.
E-mail address: shenyang.hu@pnl.gov (S.Y. Hu).

1359-6454/$36.00 © 2010 Acta Materialia Inc. Published by Elsevier Ltd. All rights reserved.
doi:10.1016/j.actamat.2010.08.020

of partial dislocations with the same Burgers vectors. In the present work we assume that twin nucleation, growth and de-twinning is a process of partial dislocation nucleation and slip on successive habit planes under internal and external stresses. A phase field model is proposed to describe the dynamics of partial dislocations and to study both stress-induced partial dislocation nucleation and twin structure evolution. Compared with atomistic simulation methods, the main advantage of the mesoscale phase field method is that it permits simulations at relatively large length and long time scales. Furthermore, it is possible to incorporate the effect of long-range elastic interactions on deformation twin evolution due to second phases, such as inclusions/precipitates, once the elastic constants and lattice mismatches are known. The capability of our model is demonstrated by modeling twin microstructure evolution in a polycrystalline fcc solid.

2. Phase field model

Fig. 1 illustrates the formation of the thinnest possible twin in the matrix formed by the nucleation and passage of three partial dislocation loops on successive planes. Since the partial dislocation is the smallest unit cell in the twin structure, we study twin evolution using partial dislocation dynamics similar to the phase field model of dislocation dynamics [18–20]. In this work an arbitrary fcc crystal is used as an example. With the assumption that a twin consists of partial dislocations with the same Burgers vectors there are 12 twin variants in a single fcc crystal related to 12 distinct partial dislocations with slip planes $\{1\,1\,1\}$ and dislocation Burgers vectors $\langle 1\,1\,\bar{2}\rangle$, respectively. Twelve order parameters $\eta_{\alpha\beta}(r, t)$ ($\alpha = 1,2,3,4$; $\beta = 1,2,3$) are used to describe the partial dislocations and their time evolution, where α denotes the four $\{1\,1\,1\}$ slip planes and β denotes the three Burgers vectors on each of the slip planes. Considering a partial dislocation loop, the discontinuous displacement across the slip plane is described as $\mathbf{u} = \eta_{\alpha\beta}(r, t)\mathbf{b}_{\alpha\beta}$, where $\mathbf{b}_{\alpha\beta}$ is the partial dislocation Burgers vector. The order parameter $\eta_{\alpha\beta}(r, t)$ is equal to 1 inside the partial dislocation loop (or in the stacking fault) and $\eta_{\alpha\beta} = 0$ outside the partial dislocation loop (outside of the stacking fault). The order parameter $\eta_{\alpha\beta}$ changes smoothly from 0 to 1 across the dislocation core. Since dislocation density is proportional to the gradient of the discontinuous displacement, the partial dislocation in the phase field model is described by distributed small dislocations, as in the Peierls–Nabarro model [21]. Such a description correctly gives the dislocation stress field far from the dislocation core and removes the non-physical singular stress in the theoretical solution. Next we discuss the energy change of the system during partial dislocation formation, glide and twin growth. The energy change includes crystalline energy, interfacial energy and elastic energy.

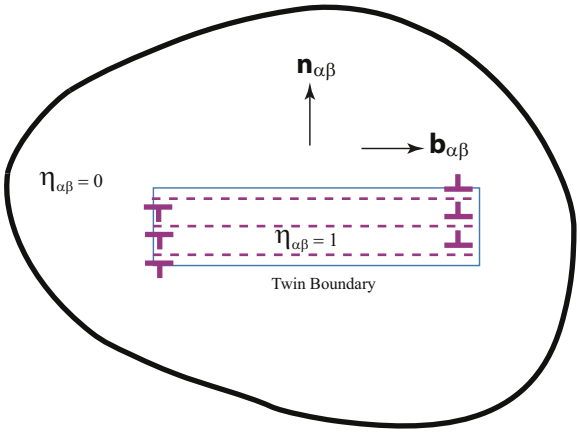

Fig. 1. A schematic view of a twin nucleus.

2.1. Crystalline energy

The twin formation in Fig. 1 involves the generation and slip of three partial dislocation loops on successive planes. The nucleation and slip of a partial dislocation loop accompanies energy changes, including crystalline energy, stacking fault energy, elastic energy, and the core energy of two partial dislocations. The crystalline energy is the energy barrier which a partial dislocation must overcome during slip. Fig. 2a, which is reproduced from the first principles calculation for Al [12], shows the energy pathway during the formation of an infinite stacking fault or a partial dislocation loop in which the two partial dislocations are separated by an infinite distance. The energy pathway does not include the elastic and core energies of two partial dislocations. The horizontal axis of the figure is exactly the same as the order parameter $\eta_{\alpha\beta}$ in our phase field model. It can be seen that the energy pathway has two local minima at the perfect crystal $\eta_{\alpha\beta} = 0$ and the crystal with infinite stacking fault $\eta_{\alpha\beta} = 1$ (or an infinite partial dislocation loop). The energy of the perfect crystal at $\eta_{\alpha\beta} = 0$ is 0 and is taken as the reference state. The energy at $\eta_{\alpha\beta} = 1$ is equal to the stacking fault energy. Fig. 2b shows the energy pathway during the formation and growth of an infinite twin [12]. When $\eta_{\alpha\beta} \leqslant 1$ the energy pathway is the same as that shown in Fig. 2a. However, when $\eta_{\alpha\beta} > 1$ the energy pathway plots the energy change during the passage of partial dislocations on successive planes. Comparing the energy changes of one stacking fault, two stacking faults and a twin structure shown in Fig. 2a and b, it was found that the stacking fault energy is very close to the energy of two twin boundaries. If we view the stacking fault energy as the interfacial energy of the partial dislocation or twin boundaries, the crystalline energy of a partial dislocation can be obtained by subtracting the stacking fault energy from the energy pathway as shown in Fig. 3. Fig. 3b plots the crystalline energy $f(\eta_{\alpha\beta})$ of the partial dislocation by subtracting $\gamma_{st}\eta_{\alpha\beta}$ from Fig. 3a, which is for a stacking fault. Such a double well potential can also be obtained by subtracting $2\gamma_{\text{twin}}$ from the energy change ($i < \eta_{\alpha\beta} < i + 1$, $i \geqslant 1$) shown in Fig. 2b.

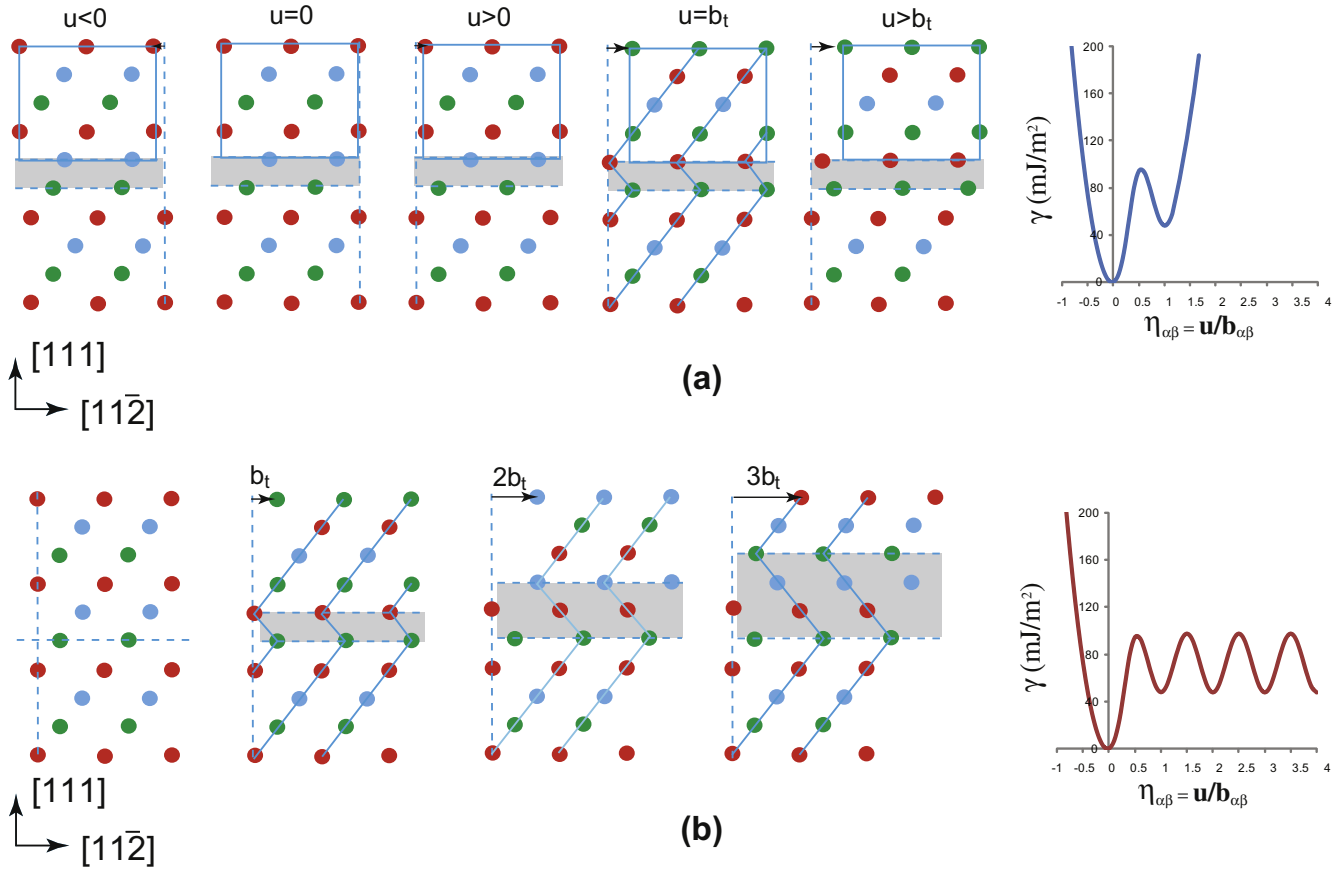

Fig. 2. Reproduced energy pathways from Kibey et al. [12]: (a) for the formation of a stacking fault and (b) for the formation of a twin.

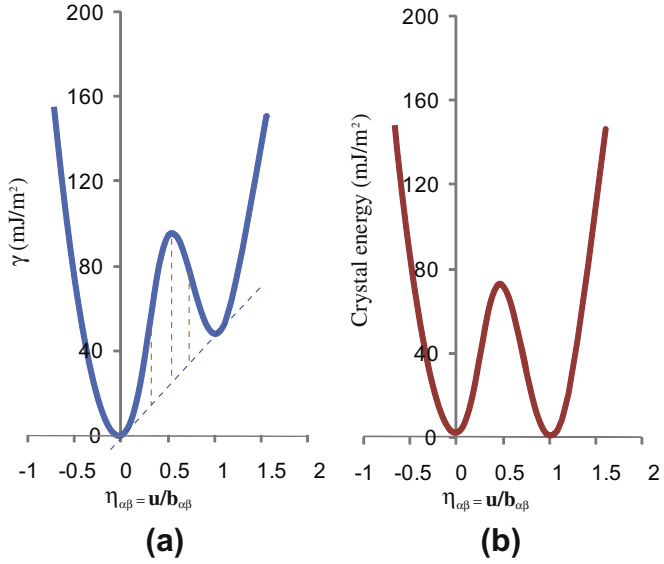

Fig. 3. (a) The energy pathway for the formation of a stacking fault and (b) the crystalline energy of a single partial dislocation.

In this work we focus on the nucleation of partial dislocations as well as twinning. Kibey et al. [12] presented a hierarchical, multi-scale theory to predict the critical twinning stress in Al. A continuous mechanical model [3] also demonstrated that the resolved shear stress in the direction of the twin Burgers vector on the habit plane controls twin nucleation. Here we assume that the nucleation and glide of partial dislocations is a process of crystal stability modification when the resolved shear stress is larger than the critical shear stress for the given crystal. We write the crystalline energy as a function of discontinuous displacement $\eta_{\alpha\beta}$ and local shear stress $\tau_{\alpha\beta}$ in the direction of the Burgers vector on the habit plane as

$$f(\eta_{\alpha\beta},\tau_{\alpha\beta}) = \sum_{\alpha,\beta}\left[A_1\eta_{\alpha\beta}^2 + A_2\eta_{\alpha\beta}^3 + A_3\eta_{\alpha\beta}^4\right] + \tau_{ss}[B_1(\eta_{\alpha\beta}-0.5) + B_2(\eta_{\alpha\beta}-1.0)^2 + B_3(\eta_{\alpha\beta}-0.5)^3 + B_4(\eta_{\alpha\beta}-0.5)^5] + \sum_{\alpha,\beta}\sum_{\alpha'\neq\alpha,\beta'\neq\beta} D\eta_{\alpha\beta}^2\eta_{\alpha'\beta'}^2 \quad \text{when} \quad \tau_{ss} \geq 0 \tag{1a}$$

$$f(\eta_{\alpha\beta},\tau_{\alpha\beta}) = \sum_{\alpha,\beta}[A_1\eta_{\alpha\beta}^2 + A_2\eta_{\alpha\beta}^3 + A_3\eta_{\alpha\beta}^4[+\tau_{ss}[B_1(\eta_{\alpha\beta}-0.5) + B_2(\eta_{\alpha\beta})^2 + B_3(\eta_{\alpha\beta}-0.5)^3 + B_4(\eta_{\alpha\beta}-0.5)^5] + \sum_{\alpha,\beta}\sum_{\alpha'\neq\alpha,\beta'\neq\beta} D\eta_{\alpha\beta}^2\eta_{\alpha'\beta'}^2 \quad \text{when} \quad \tau_{ss} \leqslant 0 \tag{1b}$$

where A_i, B_i and D are constants. The crystalline energy includes three terms. The first term is the energy pathway for

the formation of a partial dislocation as shown in Fig. 3b. This energy term describes the two phase equilibrium between a perfect crystal ($\eta_{\alpha\beta}=0$) and a crystal with a partial dislocation ($\eta_{\alpha\beta}=1$), the energy barrier to the formation of a partial dislocation and the symmetry of the crystal, i.e. uniquely identifies 12 partial dislocations in a fcc crystal. The second term describes the stability of a perfect crystal and a partial dislocation under stresses. Applied stresses and the nucleation of partial dislocations produce deformation energy. As we know, the nucleation of a partial dislocation involves a large deformation that includes two parts. One is the elastic deformation energy. The elastic energy associated with the lattice mismatch due to the partial dislocation and applied stresses/strains is included in the total energy, and calculated by solving the elastic solution, as will be discussed in the following section. The other part is the plastic deformation energy. In this work we include the plastic deformation energy in the crystalline energy and simply assume that it is proportional to the total shear stress $\tau_{\alpha\beta}$. The third term includes the interaction energy among partial dislocations with different Burgers vectors in the crystalline energy. D is a positive constant, which implies that two partial dislocations with different Burgers vectors located on the same atomic plane are energetically unfavored. Our simulation results will demonstrate that such a description of crystalline energy can reasonably capture the main thermodynamic properties of a system. Fig. 4a plots the change in crystalline energy near a perfect crystal ($\eta_{\alpha\beta}=0$) for different shear stress values τ_{ss}, which is normalized by the critical shear stress $\tau_{ss}=\tau_{\alpha\beta}/\tau_{\text{crit}}$. The shear stress is calculated as $\tau_{\alpha\beta}=\frac{\mathbf{b}_{\alpha\beta}}{|b_{\alpha\beta}|}\cdot(\sigma_{ij})\cdot\mathbf{n}_{\alpha\beta}$ where (σ_{ij}) is the local stress tensor. The crystalline energy shows that the perfect crystal ($\eta_{\alpha\beta}=0$) becomes unstable when the local shear stress is larger than the critical shear stress ($\tau_{ss}\geqslant 1$) and it may transform to a partial dislocation ($\eta_{\alpha\beta}=1$). Fig. 4b plots the change in crystalline energy near a partial dislocation ($\eta_{\alpha\beta}=1$) for different shear stress values τ_{ss} The partial dislocation will become unstable and transform back to a perfect crystal when the shear stress is larger than the critical shear stress ($\tau_{ss}\leqslant -1$). The minus sign means that the shear stress is applied in the opposite direction to the Burgers vector on the habit plane. The theoretical twinning stress $\tau_{\text{crit}}=1.94$ GPa for fcc Al [12] is used in the present work as a reasonable value.

2.2. Interfacial energy

As shown in Fig. 1, a twin made up of three partial dislocation loops has two kinds of interfaces. One is the twin boundary related to the stacking fault and the other is the end of the twin related to the distributed dislocation cores. The interfacial energy along the twin boundary is much smaller than the interfacial energy at the twin end, which depends on the type of dislocation, i.e. edge, screw or mixed dislocation. Generally speaking, these interfacial energies of a twin changes during twin evolution because the dislocation type changes along the twin ends. For simplicity, we only consider the strong anisotropy of twin interfacial energy. In order to describe the strong anisotropic interfacial energy we separate the interfacial energy into two parts as

$$E^{\text{int}}=\sum_{\alpha,\beta}\frac{\kappa}{2}\left|\nabla\eta_{\alpha\beta}\right|^2+\sum_{\alpha,\beta}\frac{\kappa_1}{2}\left|\mathbf{n}_{\alpha\beta}\times\nabla\eta_{\alpha\beta}\right|^2 \tag{2}$$

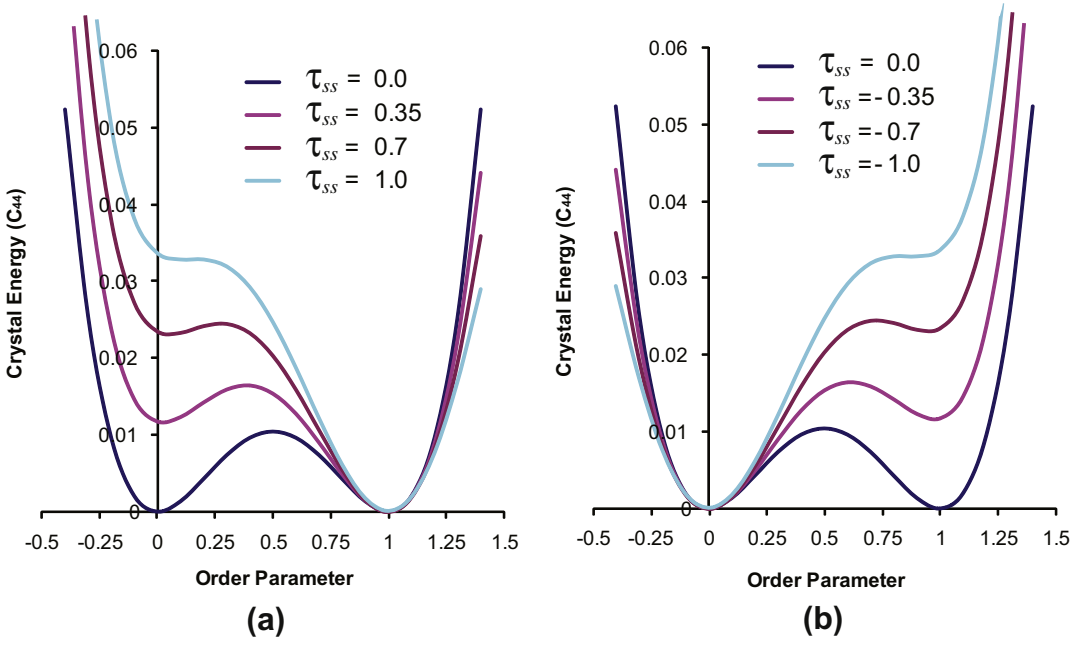

Fig. 4. Crystalline energy of partial dislocation as a function of resolved shear stress τ_{ss} in units of critical shear stress $\tau_{\text{crit}}=1.94$ GPa. C_{44} is the crystal shear modulus. (a) Perfect crystal and (b) partial dislocation.

The first term describes the twin boundary energy. The coefficient κ is determined by the twin boundary energy and the twin boundary thickness. It can be estimated as $\kappa \approx \gamma^2/\Delta f$. γ is the twin boundary energy. Δf is the height of the double well shown in Fig. 4 when $\tau_{ss} = 0$. The second term describes the interfacial energy at the twin ends, where $\mathbf{n}_{\alpha\beta}$ is the normal of the habit plane of twin variant $\eta_{\alpha\beta}$ and is 0 on the twin boundary because $\mathbf{n}_{\alpha\beta}$ and $\nabla\eta_{\alpha\beta}$ are parallel vectors. The coefficient κ_1 is determined by the dislocation core energy and dislocation core size at the ends of the twin. The dislocation core energy $\gamma_{\text{dis}}(\text{eV/Å})$ can be calculated using atomistic simulations [22–24]. The coefficient κ_1 can be estimated as $\kappa_1 \approx \gamma_{\text{dis}} r_0/d_0$, where r_0 is the dislocation core radius and d_0 is the interplanar distance of the dislocation slip plane.

2.3. Elastic energy

Using the "eigenstrain" concept [25,26], the lattice mismatches associated with partial dislocations can be described as an eigenstrain tensor as:

$$\varepsilon^d_{ij}(\boldsymbol{r}) = \sum_{\alpha,\beta} \frac{b_{\alpha\beta(i)} n_{\alpha\beta}(j) + b_{\alpha\beta}(j) n_{\alpha\beta}(i)}{2d_0} \eta_{\alpha\beta}(\boldsymbol{r}) \tag{3}$$

where $b_{\alpha\beta}(i)$ is a component of the Burgers vector, $n_{\alpha\beta}(j)$ is a component of the unit vector normal to the slip plane α, d_0 is the interplanar distance of the slip planes and the field variables $\eta_{\alpha\beta}$ are given in units of $|\mathbf{b}_{\alpha\beta}|$. The elastic energy density E^{elast} can be calculated as [36]:

$$E^{\text{elast}} = \frac{1}{2}\lambda_{ijkl}\varepsilon^{el}_{ij}\varepsilon^{el}_{kl} \tag{4}$$

using the conventional summation convention where λ_{ijkl} the stiffness tensor and ε^{el} is the elastic strain.

$$\varepsilon^{el}_{ij} = \bar{\varepsilon}_{ij} + \delta\varepsilon_{ij}(\boldsymbol{r}) - \varepsilon^d_{ij}(\boldsymbol{r}) \tag{5}$$

where $\bar{\varepsilon}_{ij}$ is the homogeneous macroscopic strain characterizing the macroscopic shape and volume change, $\delta\varepsilon_{ij}(\boldsymbol{r})$ is the heterogeneous strain, $\varepsilon^d_{ij}(\boldsymbol{r})$ is the eigenstrain associated with the dislocation distribution and δ_{ij} is the Kronecker δ. For elastic inhomogeneous solids, such as polycrystalline materials, the elastic solution can be obtained using an iteration method [27].

2.4. Total energy of the system

The total energy of the system includes the crystalline energy, interfacial energy and elastic energy terms:

$$\begin{aligned} F &= \int_\Omega \int \left[f(\eta_{\alpha\beta}, \tau_{\alpha\beta}) + E^{\text{int}} + E^{\text{elast}} \right] dv \\ &= \int_\Omega \int \left[f(\eta_{\alpha\beta}, \tau_{\alpha\beta}) + \sum_{\alpha,\beta} \frac{\kappa}{2} |\nabla\eta_{\alpha\beta}|^2 + \sum_{\alpha\beta} \frac{\kappa_1}{2} \right. \\ &\quad \left. |\mathbf{n}_{\alpha\beta} \times \nabla\eta_{\alpha\beta}|^2 + \frac{1}{2}\lambda_{ijkl}\varepsilon^{el}_{ij}\varepsilon^{el}_{kl} \right] dV \end{aligned} \tag{6}$$

If the system is an fcc polycrystal, then we can either use 12 different order parameters for each grain or we can use 12 global order parameters, but the elastic constants $\lambda_{ijkl}(r)$, the habit plane normal $\mathbf{n}_{\alpha\beta}(r)$ and the Burgers vectors $\mathbf{b}_{\alpha\beta}(r)$ should be defined locally. In this work 12 global order parameters have been used.

2.5. Kinetic equations

The evolution rate of the order parameters is assumed to be a linear function of the thermodynamic driving forces. The simplest form of the kinetic equation is the time-dependent Ginzburg–Landau equation [28]:

$$\frac{\partial\eta_{\alpha\beta}}{\partial t} = -L\frac{\delta F}{\delta\eta_{\alpha\beta}} + \xi_{\alpha\beta}(r, t) \tag{7}$$

where L is the kinetic coefficient characterizing the partial dislocation mobility, F is the total energy functional (6), $\frac{\delta F}{\delta\eta_{\alpha\beta}}$ is the thermodynamic driving force and $\xi_{\alpha\beta}(r, t)$is the Langevin Gaussian noise associated with thermal fluctuations [29]. In our model Eq. (7) is solved numerically. In order to improve the numerical stability and alleviate the constraint on the time increment for the equation we move the main part of the gradient term from the right side of Eq. (7) to the left side as [30]

$$\begin{aligned} \{\eta_{\alpha\beta} + \Delta t L\kappa\nabla^2\eta_{\alpha\beta}\}|_{t+\Delta t} = \left\{ \eta_{\alpha\beta} + \Delta t L \left(\frac{\partial f(\eta_{\alpha\beta}, \tau_{\alpha\beta})}{\partial\eta_{\alpha\beta}} \right.\right. \\ \left.\left. + \frac{\kappa_1}{2}\frac{\partial|n_{\alpha\beta}\times\eta_{\alpha\beta}|^2}{\partial\eta_{\alpha\beta}} + \sigma_{ij}\frac{\partial\varepsilon^d_{ij}}{\partial\eta_{\alpha\beta}} \right) \right\}\Bigg|_t, \end{aligned} \tag{8}$$

where Δt is the magnitude of the time increment andm σ_{ij} is the stress tensor. We use the following normalizations for the numerical calculation: $r^*_i = \frac{r_i}{l_0}, \Delta t^* = L\Delta t C_{44}$, $A^*_i = \frac{A_i}{C_{44}}$, $B^*_i = \frac{B_i}{C_{44}}, D^* = \frac{D}{C_{44}}, \kappa^* = \frac{\kappa}{l_0^2 C_{44}}$ and $\kappa^*_1 = \frac{\kappa_1}{l_0^2 C_{44}}$, with l_0 being a characteristic length, thus $\nabla = \left(\frac{\partial}{\partial r_1}, \frac{\partial}{\partial r_2}, \frac{\partial}{\partial r_3}\right) = \frac{1}{l_0}\left(\frac{\partial}{\partial r^*_1}, \frac{\partial}{\partial r^*_2}, \frac{\partial}{\partial r^*_3}\right) = \frac{1}{l_0}\nabla^*$. C_{44} is the shear modulus. In the simulations we consider fcc Al as the example, and the elastic constants are $C_{11} = 108.2$ GPa, $C_{12} = 61.2$ GPa and $C_{44} = 28.5$ GPa. Since the elastic anisotropy for Al is weak, we use the isotropic elastic constants $C_{11} = 118.3$ GPa, $C_{12} = 61.2$ GPa and $C_{44} = 28.5$ by increasing C_{11} by a small amount. The characteristic length l_0 is taken as the interplanar distance of the (1 1 1) glide planes. Eq. (8) is solved efficiently in Fourier space [30].

3. Results and discussion

To demonstrate the capability of the proposed phase field model we constructed a two-dimensional simulation cell consisting of four differently orientated grains. The orientations of grains 1–3 are shown in Fig. 5a. $\theta_i (i = 1, 2, 3)$ denotes the angle between direction $[1\,1\,\bar{2}]$ or $[0\,1\,\bar{1}]$ and the x-axis. The orientation of grain 4 was the same as grain 1, which

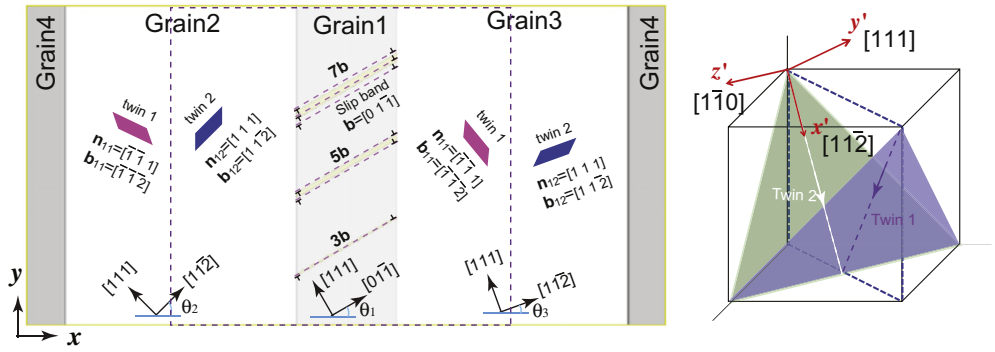

Fig. 5. (a) Schematic illustrating the orientations of grains, twins and slip bands and (b) Burgers' vectors of the two twins of interest in this work.

Table 1
The dimensionless parameters used in the simulations.

Time	Δt^*	0.01
Characteristic length	l_0	0.268 nm
Gradient coefficient	κ^*	0.0016
Gradient coefficient	κ_1^*	0.1
Elastic constants	C_{ij}^*	$C_{11}^* = 4.15$, $C_{12}^* = 1.25$, $C_{44}^* = 1.0$
Coefficients of crystalline energy	A_i^*, B_i^*, D	$A_1^* = 0.167$, $B_1^* = -0.043$ $A_2^* = -0.352$, $B_2^* = 0.010$ $A_3^* = 0.167$, $B_3^* = 0.160$ $D^* = 0.167$, $B_4^* = -0.139$
Critical shear stress of twin nucleation	$\tau_{crit}^* = \tau_{crit}/C_{44}$	0.0701
Orientations of grains and slip bands	Case 1	$\theta_1 = 0$, $\theta_2 = 45$, $\theta_3 = 0$
	Case 2	$\theta_1 = 30$, $\theta_2 = 45$, $\theta_3 = 0$
	Case 3	$\theta_1 = 0$, $\theta_2 = 45$ $\theta_3 = 30$
	Case 4	$\theta_1 = 30$, $\theta_2 = 45$, $\theta_3 = 30$

ensured that the simulation cell was periodic in the x direction. As shown in Fig. 5b, two twin variants, their habit planes perpendicular to the plane of the figure, existed in grains 2 and 3. Considering the two-dimensional simulation cell, we assumed that all twin variants in grain 1 with habit planes that were not perpendicular to the figure plane were not active in the simulations. We also assumed that there are pre-existing slip bands in grain 1 that produce internal stresses. Three slip bands, which had 3, 5 and 7 dislocations, respectively, were placed in grain 1, as shown in Fig. 5. The dislocations had Burgers vector $\mathbf{b} = [0\,1\,\bar{1}]$ and piled up on successive (1 1 1) planes at the grain boundaries. Table 1 lists the material properties and model parameters.

The dislocations in slip bands were described by the Peierls–Nabarro model with a dislocation core size of four lattice constants to eliminate stress singularity at the dislocation core [25]. The eigenstrain tensor in Eq. (3) was used to describe the lattice mismatch of the slip bands. Our previous work [31] indicated that the numerical dislocation stress solution outside the dislocation core was in good agreement with the analytical solution. Fig. 6 plots the distribution of shear stress σ_{12} produced by the slip bands in the region marked by the dashed line in Fig. 5a for two different sets of grain orientations. The purple contours show that the shear stress in the twin Burgers vector direction $\mathbf{b}_{11}$ on the habit plane $\mathbf{n}_{11}$ was equal to the critical shear stress for dislocation nucleation. This implies that twin 1 may nucleate inside the purple contours. The blue contours identify the possible nucleation region of twin 2. It can be seen that the potential nucleation regions strongly depend on the orientation and thickness of the pre-existing slip bands. In the simulations we considered four different sets of grain orientations, listed in Table 1. The simulations first examined the nucleation of partial dislocations and twins induced by the internal stresses produced by the slip

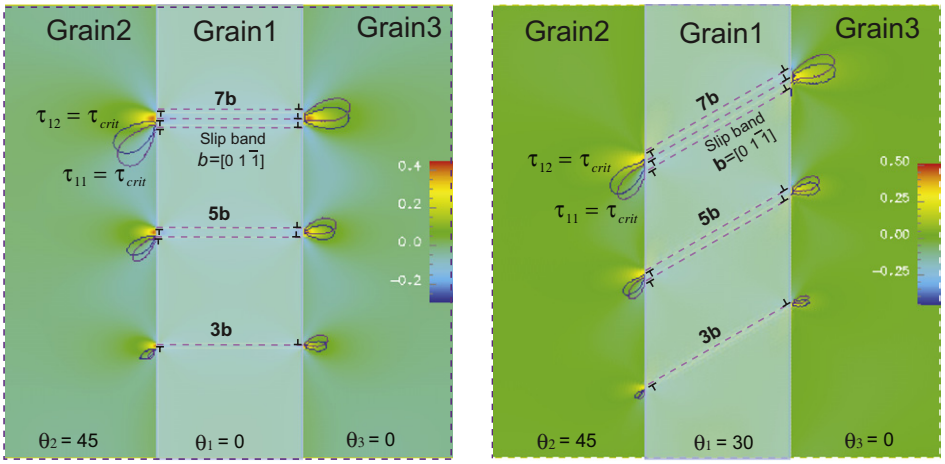

Fig. 6. Distribution of shear stress σ_{12} around slip bands. (a and b) Two different orientations of grain and slip bands.

bands, and then an increasing external strain was applied at the simulation cell, described by

$$\varepsilon_{ij}^{\mathrm{appl}} = \begin{bmatrix} -0.0016 & 0.002 & 0 \\ 0.002 & 0.0016 & 0 \\ 0 & 0 & 0 \end{bmatrix} \varepsilon_0^{\mathrm{appl}} = \begin{bmatrix} -0.0016 & 0.002 & 0 \\ 0.002 & 0.0016 & 0 \\ 0 & 0 & 0 \end{bmatrix} \dot{\varepsilon}_0 t^* \tag{9}$$

where $\dot{\varepsilon}_0$ is the strain rate and t^* is the normalized time. The applied strain tensor produces a pure shear stress, as shown in Fig. 7. A small strain rate $\dot{\varepsilon}_0 = 1/(6000\Delta t^*)$ was used to ensure that the twin nuclei and structures observed in the simulations had energetically favored morphologies, including size, shape and orientation. We used the coefficient $\varepsilon_0^{\mathrm{appl}} = \dot{\varepsilon}_0 t^*$ for the applied strain tensor to control

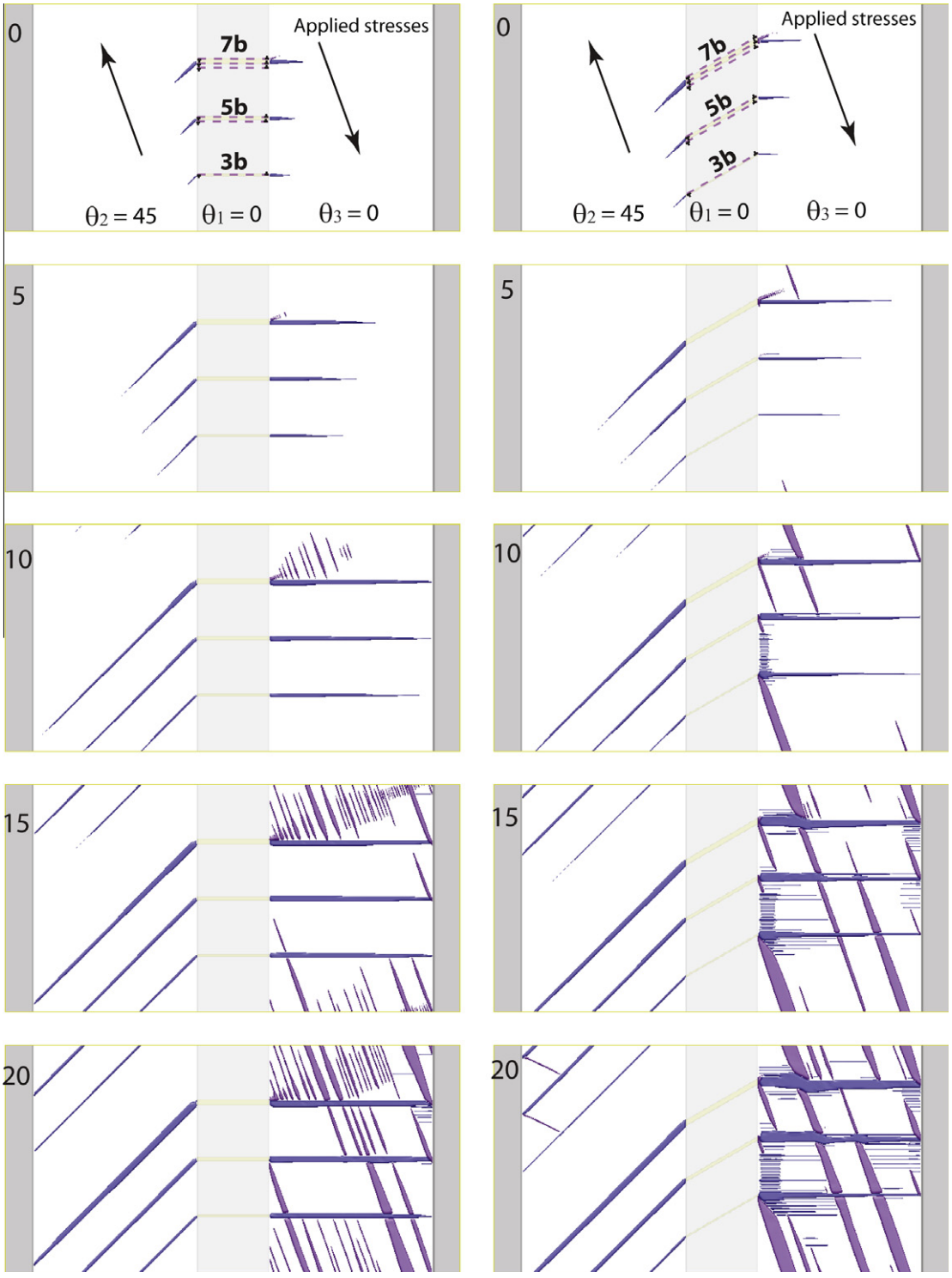

Fig. 7. Twin microstructure evolution during loading: (a) Case 1 with grain orientations $\theta_1 = 0$, $\theta_2 = 45$, $\theta_3 = 0$ and (b) Case 2 with grain orientations $\theta_1 = 30$, $\theta_2 = 45$, $\theta_3 = 0$. The numbers in the figures show the applied strain $\varepsilon_0^{\mathrm{appl}}$.

the magnitude of the applied strain. Above $\varepsilon_0^{appl} = 20$ the applied strain decreased at a rate $\dot{\varepsilon}_0 = -1/(6000\Delta t^*)$ to simulate twin evolution under mechanical unloading.

3.1. Nucleation of partial dislocations and twins

Our phase field model assumes that the nucleation of partial dislocations occurs through structural instability due to locally high shear stresses. Figs. 7 and 8 show the nucleation and evolution of partial dislocations and twins near the slip bands due to the applied strains. The value of ε_0^{appl} during loading is listed in the figures. The purple regions in grains 2 and 3 denote the partial dislocation (Burgers vector $\mathbf{b} = [\bar{1}\,\bar{1}\,\bar{2}]$ and slip plane $\mathbf{n} = [\bar{1}\,\bar{1}\,1]$) or twin 1. The blue regions in grains 2 and 3 denote twin 2. Since the characteristic length l_0 is taken as the interplanar distance of (1 1 1) planes, one

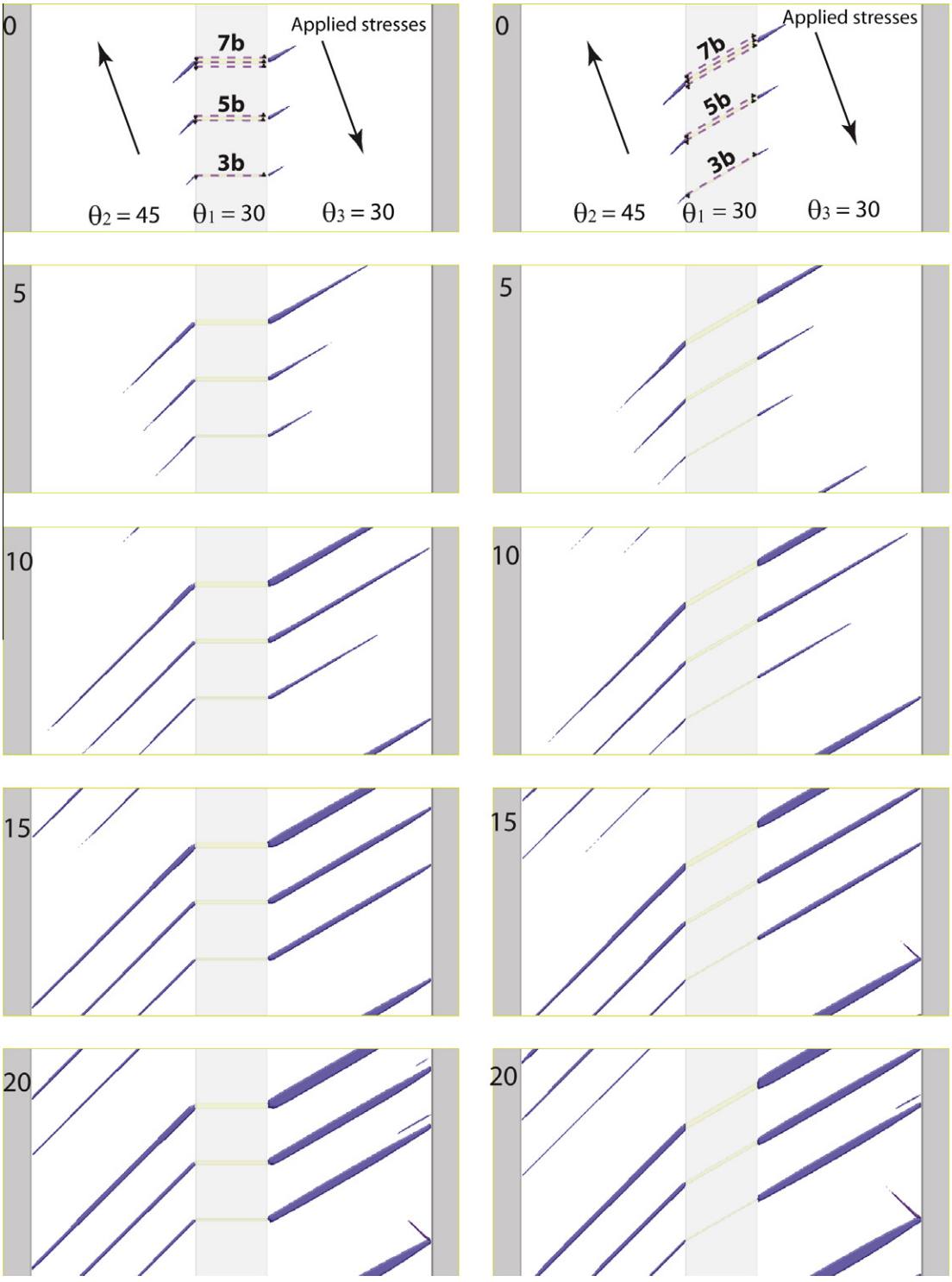

Fig. 8. Twin microstructure evolution during loading: (a) Case 3 with grain orientations $\theta_1 = 0$, $\theta_2 = 45$, $\theta_3 = 30$ and (b) Case 3 with grain orientations $\theta_1 = 30$, $\theta_2 = 45$, $\theta_3 = 30$. The numbers in the figures show the applied strain ε_0^{appl}.

step on the twin boundaries is related to one partial dislocation. Comparing the potential nucleation regions of twins around the slip bands shown in Fig. 6 and the predicted nuclei shown in Figs. 7a and 8a when $\varepsilon_0^{appl} = 0$, it was found that the sizes of the twin nuclei were much smaller than the potential nucleation regions, which can be understood if we note that the formation of a finite twin or partial dislocation loop will increase the total interfacial energy, including the twin boundary energy and dislocation core energy, and will reduce local stresses because the internal shear stress is opposite to the shear stress associated with twin formation. The shear stress distributions after the twins nucleated are presented in Fig. 9. Comparing Figs. 9 and 6, we fond that twin formation largely reduced the maximum shear stresses and modified the potential nucleation sites. From Figs. 7 and 8 at $\varepsilon_0^{appl} = 0$ it can also clearly be seen that nucleated twins included several partial dislocations with the same Burgers vector, a thicker slip band induced a larger twin and the orientations of the twins were consistent with the grain orientation. Although twin 1 was supposed to nucleate inside the purple regions, twin 1 was only observed to nucleate at thicker slip bands in Fig. 7b. It should be pointed out that no order parameter fluctuations, i.e. $\xi_{\alpha\beta},(r, t) = 0$ were applied in the simulations. This means that the nucleation of partial dislocations resulted from a modified crystal structure stability due to high local shear stresses. The twin morphology, including the orientation, shape and size, was completely determined by minimization of the crystalline energy associated with the partial dislocation, the interfacial energy associated with the twin boundaries and dislocation cores and the elastic energy related to pre-existing slip bands and the formation of twins. Therefore, we conclude that the model is able to predict the nucleation of twins and dislocations as well as the twin nucleus morphology.

3.2. Evolution of partial dislocations and twins during loading

MD simulations in nanocrystalline Al showed that the ability of grain boundaries in a nanocrystalline microstructure under high stress to nucleate partial dislocations at a high rate inevitably leads to deformation twinning [15]. Twin morphology evolution is illustrated in Figs. 7 and 8 as the applied strain increased. As expected, twin structures depended on the particular orientations of grains and slip bands. It can clearly be seen that most partial dislocations were emitted from grain boundaries, which is in agreement with the MD simulations. As a consequence, a twin structure with a broad root at the grain boundary and a narrow tip formed. Such a twin structure has been observed in Fe, as shown in Fig. 10. It can also be seen that internal stresses around the pre-existing slip bands promoted the nucleation of twin 2. However, the applied strain, which produced a shear stress on slip plane $\mathbf{n} = [\bar{1}\,\bar{1}\,1])$ in grain 3 with orientation $\theta_3 = 0$, resulted in the formation of twin 1, as shown in Fig. 7a and b.

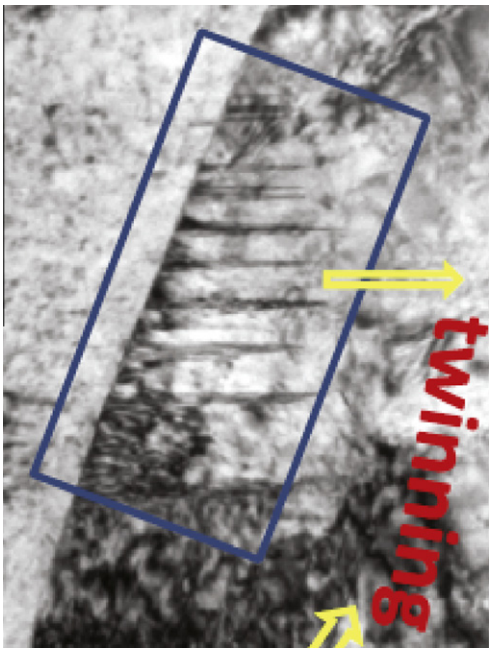

Fig. 10. TEM image of twin morphology at grain boundaries in Fe from Dr. Yufeng Shen (private communication).

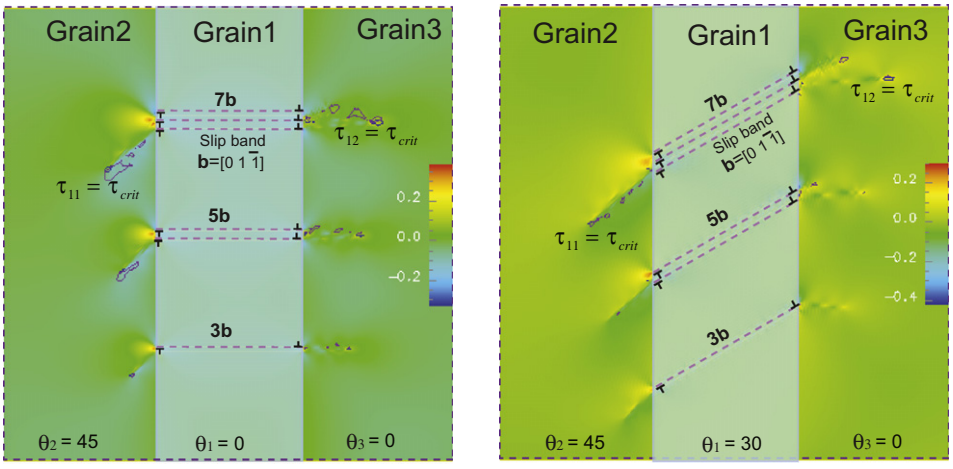

Fig. 9. Distributions of shear stress σ_{12} after twin formation around slip bands. (a and b) Two different orientations of grain and slip bands.

The results in Figs. 7 and 8 show a number of twin growth phenomena. For example, one twin cannot penetrate another twin, so continuous growth stops at the twin boundary. As a result, it may block partial dislocations slipping through or initiate partial dislocation nucleation, as shown in Fig. 7b. High local stresses may promote twin nucleation at the other side of the twin, as shown in Fig. 7a and 7b. It can be observed in Figs. 7 and 8 that a twin blocked at a grain boundary activates another twin nucleation. For two sets of grain orientations we can see that partial dislocations were continuously emitted from grain boundaries and the cross-sections of two twins in Fig. 7a and b. The results demonstrate that our model can reasonably reproduce the expected phenomena of twin evolution and describe the interaction between differently orientated twins and their growth behavior.

3.3. Evolution of partial dislocations and twins during unloading

Twin growth involves the nucleation and glide of partial dislocations. If an opposite stress is applied to the simulation cell the partial dislocations will reverse their slip direction. If the local stress is larger than the critical shear stress the partial dislocations or the stacking fault will become unstable, as shown in Fig. 4b. Fig. 11 illustrates twin and partial dislocation evolution during unloading from the microstructure shown in Fig. 7. Comparing the microstructures at $\varepsilon_0^{\text{appl}} = 20$ and $\varepsilon_0^{\text{appl}} = 15$ we observe that some partial dislocations continued their glide at the beginning of unloading, but most started to reverse their glide direction in response to the changes in local stress. With continuous unloading partial dislocations showed reverse gliding and

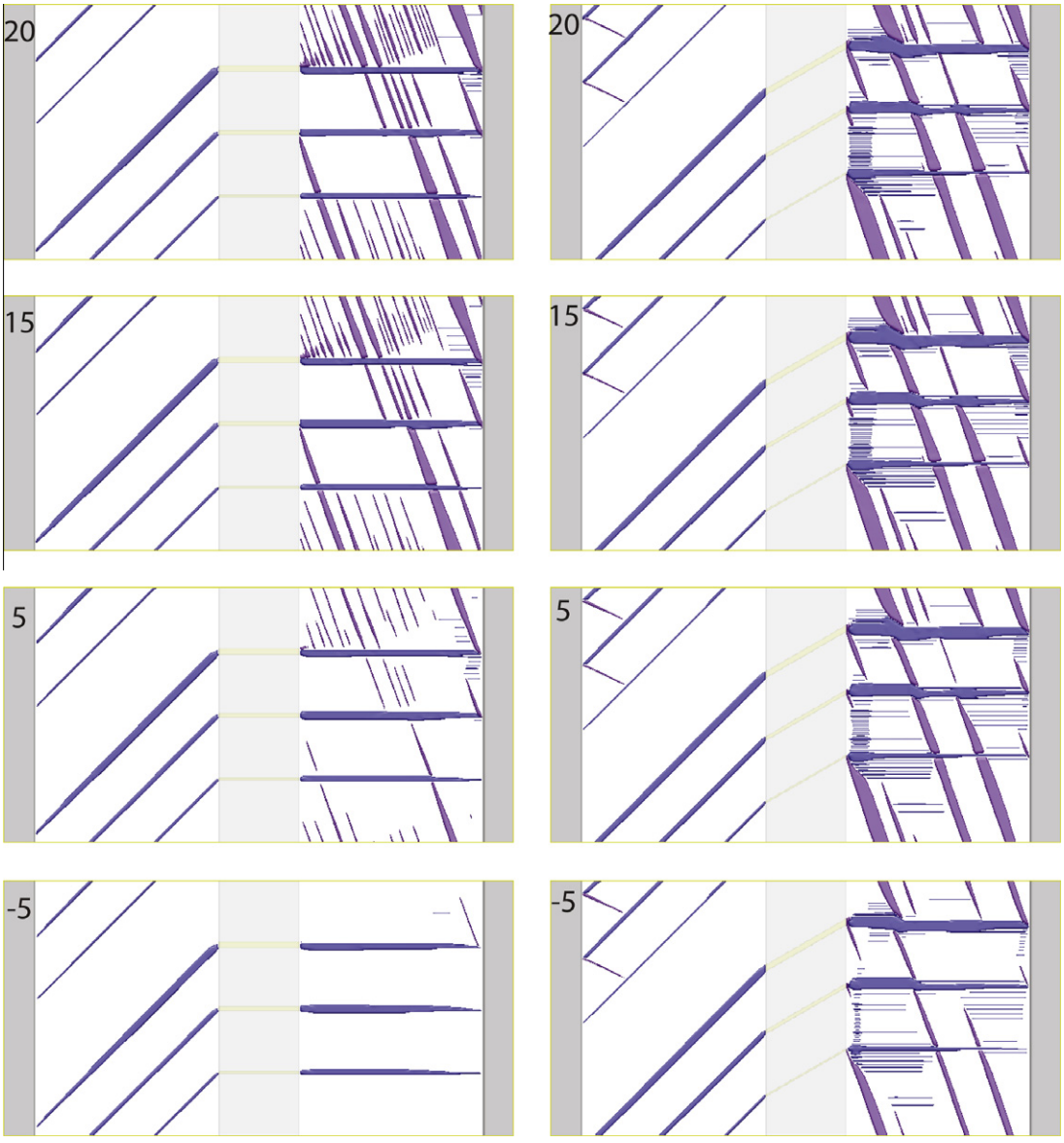

Fig. 11. Twin microstructure evolution during unloading: (a) Case 1 with grain orientations $\theta_1 = 0$, $\theta_2 = 45$, $\theta_3 = 30$ and (b) Case 2 with grain orientations $\theta_1 = 30$, $\theta_2 = 45$, $\theta_3 = 30$. The numbers in the figures show the applied strain $\varepsilon_0^{\text{appl}}$.

de-twinning took place. Experiments and MD simulations also showed de-twinning in pure Al [32]. If we carefully examine the twin structures during loading and unloading in Figs. 7 and 11 it is clear that the evolution of twin structures was not completely reversible, but rather exhibited mechanical hysteresis. In fact, we observe that a number of twins and partial dislocations remained even when the applied strain was $\varepsilon_0^{\text{appl}} = -5$. The observed mechanical hysteresis might result from stress relaxation due to nucleation and glide of partial dislocations and the presence of grain boundaries. The reverse stresses acting on twin structures are thus lower during unloading, leading to less de-twinning. The effect of stress relaxation due to grain boundaries on twinning and de-twinning has also been observed in experiments [33]. Therefore, the twin structures depend on not only the macroscale applied strains (loading history) but also the local stress relaxation due to microstructures and microstructure evolution.

4. Conclusion

In this work we have proposed, for the first time, a phase field model to predict both nucleation and evolution of twin structures in a polycrystalline material with defects and subject to external applied loads. The model was developed for fcc Al and was based on the assumption that a twin evolves via the nucleation and glide of partial dislocations. Stacking fault energies, energy pathways (γ surfaces), ideal critical shear stresses for the formation of stacking faults and dislocation core energies were used to construct a thermodynamic model for the crystalline energy of partial dislocations, twin boundary energies and critical shear stresses that determine the stability of perfect crystals and stacking faults. The model was used to simulate the nucleation of twins and partial dislocations around slip bands and grain boundaries and the evolution of twins and partial dislocations during loading and unloading. The results demonstrate that: (1) the model is able to predict the nucleation of twins and dislocations as well as the morphology of the twin nuclei; (2) the model can reasonably reproduce the expected phenomena of twin evolution and describe the interaction between differently orientated twins and their growth behavior; (3) the twin structure evolution depends on not only the external applied strains (loading history) but also local stress relaxation. The model can be used to study the effect of defects such as inclusions, voids and grain boundaries on deformation twin evolution and mechanical properties.

Acknowledgements

This research was supported by the US Department of Energy NA22 Project "Property improvement in CZT via processing and modeling innovations" in the Pacific Northwest National Laboratory, which is operated by Battelle Memorial Institute for the US Department of Energy under Contract No. DE-AC05-76RL01830. S.H. would like to thank Drs. X. Sun and Y.F. Shen at Pacific Northwest National Laboratory and Drs. Y. Wang and T.W. Heo at The Pennsylvania State University for helpful discussions.

References

[1] Mahajan S, Chin GY. Acta Metall Mater 1973;21:1353.
[2] Christian JW, Mahajan S. Prog Mater Sci 1995;39:1.
[3] Lebensohn RA, Tome CN. Philos Mag A 1993;67:187.
[4] Wu XL, Liao XZ, Srinivasan SG, Zhou F, Lavernia EJ, Valiev RZ, et al. Phys Rev Lett 2008:100.
[5] Wu XL, Narayan J, Zhu YT. Appl Phys Lett 2008:93.
[6] Zhu YT, Wu XL, Liao XZ, Narayan J, Mathaudhu SN, Kecskes LJ. Appl Phys Lett 2009:95.
[7] Zhu YT, Narayan J, Hirth JP, Mahajan S, Wu XL, Liao XZ. Acta Mater 2009;57:3763.
[8] Chen MW, Ma E, Hemker KJ, Sheng HW, Wang YM, Cheng XM. Science 2003;300:1275.
[9] Yamakov V, Wolf D, Phillpot SR, Mukherjee AK, Gleiter H. Nat Mater 2004;3:43.
[10] Rudolph P, Koh HJ, Schafer N, Fukuda T. J Cryst Growth 1996;166:578.
[11] Coleman WA, Armstrong TW. Oakridge (USA) Report, ORN 64606. Oak Ridge, TN: Oak Ridge National Laboratory; 1970.
[12] Kibey S, Liu JB, Johnson DD, Sehitoglu H. Acta Mater 2007;55:6843.
[13] Kibey S, Liu JB, Johnson DD, Sehitoglu H. Appl Phys Lett 2007:91.
[14] Kibey S, Liu JB, Curtis MJ, Johnson DD, Sehitoglu H. Acta Mater 2006;54:2991.
[15] Yamakov V, Wolf D, Phillpot SR, Gleiter H. Acta Mater 2002;50:5005.
[16] Tschopp MA, Tucker GJ, McDowell DL. Comput Mater Sci 2008;44:351.
[17] Henager CH, Hoagland RG. Philos Mag 2005;85:4477.
[18] Wang YU, Jin YM, Cuitino AM, Khachaturyan AG. Appl Phys Lett 2001;78:2324.
[19] Shen C, Wang Y. Acta Mater. 2003;51:2595.
[20] Hu SY, Li YL, Zheng YX, Chen LQ. Int J Plasticity 2004;20:403.
[21] Hirth JP, Lothe J. Theory of dislocations. New York: McGraw-Hill; 1968.
[22] Woodward C, Rao SI. Philos Mag 2001;81A:1305.
[23] Li J, Wang CZ, Chang JP, Cai W, Bulatov VV, Ho KM, et al. Phys Rev B 2004:70.
[24] Cai W, Bulatov VV, Chang JP, Li J, Yip S. Phys Rev Lett 2001;86:5727.
[25] Mura T. Micromechanics of defects in solids. Amsterdam: Martinus Nijhoff; 1982.
[26] Khachaturian AG. Theory of structural transformations in solids. New York: Wiley Interscience; 1983.
[27] Hu SY, Chen LQ. Acta Mater 2001;49:1879.
[28] Allen SM, Cahn JW. J Phys 1977;38:C7.
[29] Gunton JD, Miguel MS, Sahni PS. Phase Transitions and Critical Phenomena. In: Domb C, Kebowitz JL, editors. New York: Academic Press; 1983. p. 267.
[30] Chen LQ, Shen J. Comput Phys Commun 1998;108:147.
[31] Hu SY, Chen LQ. Acta Mater 2001;49:463.
[32] Li BQ, Sui ML, Li B, Ma E, Mao SX. Phys Rev Lett 2009:102.
[33] Muransky O, Barnett MR, Carr DG, Vogel SC, Oliver EC. Acta Mater 2010;53:1503.